

Design of a High-Throughput Chemical Trace Detection Portal That Samples the Aerodynamic Wake of a Walking Person

Brent A. Craven, Michael J. Hargather, Jason A. Volpe, Stephen P. Frymire, Gary S. Settles

Abstract—The aerodynamic wake behind a walking person is first investigated using flow visualization and spectrophotometry in order to characterize the plume-to-wake transition and the decay of a trace body contaminant downstream of a walking human. The buoyant human thermal plume is shown to transition to an aerodynamic wake at a walking speed of approximately 0.25 m/s. At higher walking speeds the human wake is highly turbulent, resulting in an exponential decay of a passive scalar downstream of the walking human subject. From these results, a high-throughput chemical trace detection portal that uses the natural momentum of the wake to assist its collection is designed. This wake collection portal is shown to be capable of substantial improvement in security-checkpoint throughput over previous trace-detection-screening technology. To collect and sample the trace-bearing wake for a chemical signal, air flow rates nearly an order of magnitude larger than those of the previous collection technology must be accommodated. A high-flow-rate particle impactor was designed and tested to effectively collect the entire human aerodynamic wake. This impactor accommodates a flow rate of 750 L/s with a particle cutoff diameter of 5 μm . An iterative CFD process is described which streamlined the impactor geometry to reduce the total pressure drop across it. Experimental results are presented on the impactor collection efficiency. Preliminary experimental results show that trace chemicals can be detected at a useful level from a range of locations across the body when a human subject passes through the system wearing a chemical particle patch source.

I. INTRODUCTION

As a result of thermoregulation, the human body core temperature remains relatively constant at 37° C [1, 2]. This produces an elevated body surface temperature that heats ambient air next to the body, leading to a rising free-convection thermal boundary layer that begins at the feet. Initially, the boundary layer is laminar; however, as the flow proceeds up the legs, transition occurs and the upper body becomes

enveloped in turbulent flow. At moderate room temperatures and with ordinary levels of activity, this typically occurs at approximately chest height [3]. At the shoulders, the boundary layer separates and a region of recirculation forms. The separated flow above the shoulders then mixes with the buoyancy-driven flow from the head and rises above the body to form what is known as the *human thermal plume*. Experiments and computational fluid dynamics (CFD) simulations have shown that the maximum plume velocity is about 0.2 – 0.3 m/s and plume flow rates are in the 20 – 80 L/s range, depending on activity levels, height above the human subject, and characteristics of the indoor environment (room height, thermal stratification, etc.) [3].

Lateral motion between a person and the air may be due to a breeze or to walking through still air. In either case, the overall effect of free convection about the body is diminished and the human thermal plume bends over at an angle with respect to the flow direction.

The theoretical criterion for the boundary between free and forced convection is: $Gr/Re^2 \sim 1$, where Gr and Re are the non-dimensional Grashof and Reynolds numbers, respectively [4]. Thus, as the freestream velocity increases (as a person walks faster), the flow about the body becomes dominated by horizontal forced convection and the temperature difference between the body and the air ceases to be relevant. At this point, the term “human thermal plume” is dropped and the flow now is called the “human aerodynamic wake.”

Using an average body surface temperature of 26.6° C [3] and a characteristic length scale of 0.58 m (the shoulder width of a typical person. Also a representative length for the hip-to-shoulder development of the thermal boundary layer about a walking human [5]), the critical walking speed at which $Gr/Re^2 \sim 1$ occurs is estimated to be roughly 0.3 m/s. This is comparable to the maximum upward speed of the human thermal plume in a uniform environment [3], and to the value developed by Rapp [6]. Thus, for walking speeds above approximately 0.3 m/s, forced convection is expected to dominate the flow, and the human thermal plume transitions to an aerodynamic wake.

The human aerodynamic wake is the unsteady airflow downstream of a walking person (or a motionless person standing in a breeze). At typical walking speeds of 1 – 2 m/s ($Re = 37 \times 10^3 - 75 \times 10^3$, based on a characteristic shoulder width of 0.58 m [5]) flow separation occurs on the body, leading to a fully-turbulent downstream wake. Experiments [7, 8] and CFD simulations [5] have shown that the human

B. A. Craven (bac207@psu.edu) is the Head of the Computational Methods Development Department at the Applied Research Laboratory, Pennsylvania State University, University Park, Pennsylvania, 16802

M. J. Hargather (mjh@nmt.edu) is an Assistant Professor in the Mechanical Engineering Department, New Mexico Tech, 801 Leroy Place, Socorro, New Mexico, 87801

J. A. Volpe (jason.a.volpe@gmail.com) is a Product Development Engineer with North American Specialty Products, Wayne, Pennsylvania, 19807

S. P. Frymire (steve.frymire@gmail.com) is a Senior Engineer at Knolls Atomic Power Laboratory, Niskayuna, New York, 12309

G. S. Settles (gss2@psu.edu) is a Distinguished Professor of Mechanical Engineering, in the Department of Mechanical and Nuclear Engineering, The Pennsylvania State University, 208 Reber Building, University Park, Pennsylvania, 16802

All authors were employees of Pennsylvania State University when their respective contributions were made to this work.

wake is comprised of three distinct regions: the near-wake behind the torso, the near-wake behind the legs, and the far-wake. The near-wake behind the torso is distinguished by a large vortical recirculation region, with Kármán-street-type alternate left-right vortex shedding, and by the presence of downwash behind the head that was observed to laterally spread to the lower regions of the wake. The near-wake behind the legs is dominated by a jet-type flow that originates between the legs. Lastly, the far-wake is located at distances greater than about two body widths downstream, where entrainment by large-scale turbulent structures causes the width of the wake to spread and mix out in the downstream direction [5].

Due to turbulent mixing, a contaminant released on the human body will thoroughly mix within the wake and will rapidly become diluted [9]. In experiments by Cohen and Director [10], the concentration of a passive scalar in the wake of a two-dimensional bluff body decreased exponentially with time, which may be related to distance via Taylor's hypothesis [11]. They also concluded that shed vortices have a significant influence on the dispersion of a passive scalar in the near-wake. Numerical simulations of the human wake have shown that, although the concentration of a body contaminant tends to be slightly higher within the shed vortices, turbulent mixing is so rapid that the concentration in the wake at a given downstream distance is nearly spatially uniform [9, 5].

II. OBJECTIVES

The primary objective of this study is to develop a novel device to collect and sample the human aerodynamic wake for trace chemical contamination. First, the human aerodynamic wake is further characterized via experimental measurements of the plume-to-wake transition and the decay of a body contaminant downstream of a walking person. Given these data and knowledge of the fluid dynamics of the human wake from previous studies, we then design a wake collection system that utilizes the inherent momentum of the wake as a means for its collection and a custom high-flow-rate particle impactor to sample the wake for trace particle contamination. Details of the design process are presented here, culminating in the development and preliminary testing of a walk-through chemical trace detection "portal." Compared with existing technology that relies on the buoyancy-driven human thermal plume as a non-intrusive means for chemical trace detection (e.g., [12]), the present design promises to significantly reduce the time required to interrogate a person for trace contamination, thereby permitting high-throughput security screening, as one application example.

III. FURTHER CHARACTERIZATION OF THE HUMAN AERODYNAMIC WAKE

To properly design a chemical trace detection portal that samples the aerodynamic wake of a walking person, two additional pieces of information are required beyond existing knowledge of the fluid dynamics of the human wake (reviewed in Section I): validation of the theoretical walking speed at which the human thermal plume transitions to an aerodynamic wake, and an experimental characterization of the decay of

a body contaminant in the human wake. The following two sections describe experimental measurements conducted to characterize these phenomena.

A. Plume-to-Wake Transition

The plume-to-wake transition was visualized using a 1.0-meter-aperture double-pass coincident schlieren system [13]. The schlieren technique visualizes refractive index gradients, here allowing the visualization of the human thermal plume and its transition to the human aerodynamic wake. Video of a human subject was recorded at various walking speeds in otherwise-still air, and representative images at four different speeds are shown in Fig. 1(a). Such images were used to measure the approximate angle of the leading edge of the plume, which is plotted versus walking speed in Fig. 1(b). Defining the plume-to-wake transition as the change in trend between low- and high-speed relative motion, we conclude that this phenomenon occurs at approximately 0.2 m/s, which is consistent with the foregoing theoretical estimate. Thus, though there will be some variation depending on an individual's clothing, height, shoulder width, etc., the buoyant human thermal plume is dominant below a walking speed of roughly 0.2 m/s, and above it the thermal plume transitions to a momentum-dominated aerodynamic wake.

B. Body Contaminant Decay in the Human Wake

The decay of a body contaminant was measured experimentally using spectrophotometry. To seed the human aerodynamic wake with a uniformly-distributed body contaminant, our subject (male volunteer, 1.78 m tall, weighing 90.7 N [200 lb], shoulder width of 0.58 m, used for all experiments except the previous plume-to-wake-transition measurements) stood in a $0.23 \times 0.29 \times 0.44$ m rectangular box into which theatrical fog was injected from a LeMaitre G100 theatrical fog generator at a fog production rate of about $1 \text{ cm}^3/\text{s}$ for approximately 10 seconds. This box served as a plenum or chamber from which the human boundary layer entrained theatrical fog, consisting of liquid particles of approximately $5 \text{ }\mu\text{m}$ in diameter [3]. Then, as the seeded free-convection boundary layer developed about the body of the subject, it became thoroughly "contaminated" by these theatrical fog particles, which are believed to collectively behave as a passive scalar.

As shown in Fig. 2(a), once the human boundary layer was adequately seeded with theatrical fog, the subject stepped from the box and began walking at a target walking speed of 1.34 m/s (3 miles/hour, a fast walk) toward the experimental test area, located 3 m away. For all experiments in this study (including those in subsequent sections), a walking speed of 1.34 m/s ($Re = 50 \times 10^3$, based on a characteristic shoulder width of 0.58 m) was used. This was determined to be a fast but "comfortable" pace, as expressed by our experimental subject. Further, according to Human Factors personnel of the Transportation Security Administration (TSA), the average walking speed of a typical airport passenger is 1.1 m/s [14]. Even so, Moyer showed that, at walking speeds as slow as 0.7 m/s, there is no noticeable difference in the phenomenology

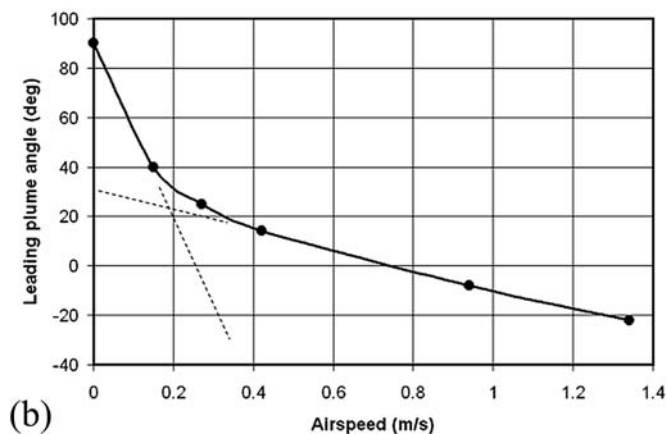
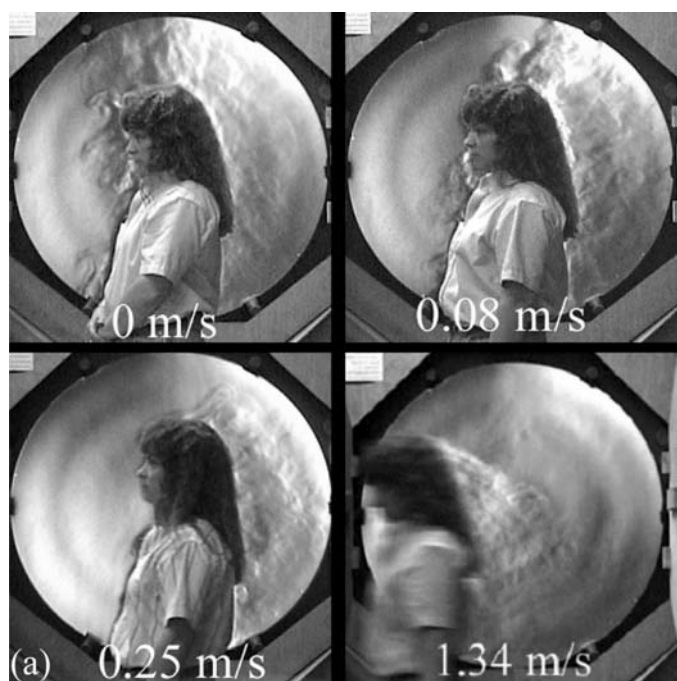


Fig. 1. (a) Representative schlieren images of a human subject walking at various speeds, (b) Data extracted from the plume-to-wake visualization experiments showing the variation in the angle of the plume leading edge as a function of walking speed.

of the human aerodynamic wake [7]. Furthermore, Moyer concluded that arm motion has virtually no effect on the physics of the wake. Nonetheless, to eliminate variable arm motion, our human subject was instructed to keep his arms next to his torso while walking, for all experiments.

The speed of the subject was monitored using two sets of 1.0-milliwatt helium-neon lasers and photodiodes that were positioned transverse to the subject's walking path. As the subject walked toward the experimental test area, the time taken to traverse the twin laser beams was recorded, yielding a measurement of the subject's walking speed. Figure 2(b) shows a representative histogram of the subject's walking speed, where the subject achieved an average speed of 1.34 m/s with a standard deviation of 0.05 m/s. In all such experiments, laser eye protection was provided to the human subject.

Using the second helium-neon laser and photodiode, which

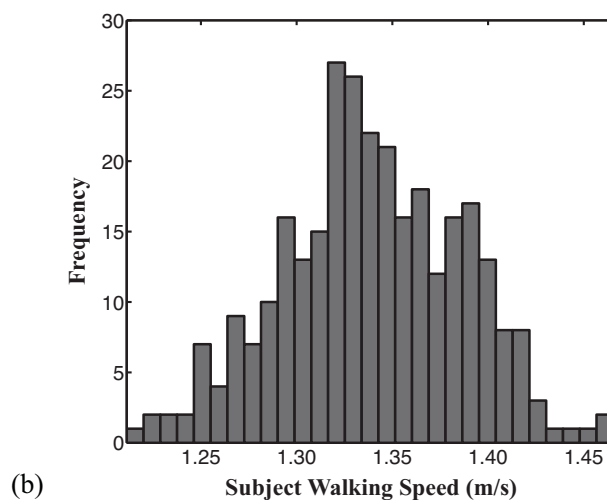
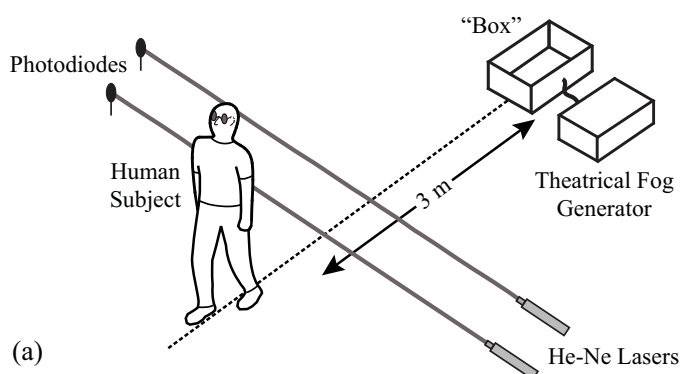


Fig. 2. (a) Schematic illustration of the human aerodynamic wake body contaminant decay experimental setup. (b) Representative histogram of subject walking speed across 300 individual experiments in the present study.

were positioned 2.75 m apart, 3 m from the box at a height of 1.04 m from the floor (approximately mid-torso height), the spectrophotometric technique [15] was utilized to measure the decay of a body contaminant in the human wake. Specifically, as the subject walked through the 2-mm diameter laser beam, the variation in transmitted laser light intensity through the contaminant-laden wake to the photodiode, was recorded. The presence of the human subject was signaled by the complete blockage of the laser beam. The instant when the laser light became no longer obstructed by the human subject was then chosen as the zero-time for the experiments, as shown in Fig. 3. To obtain a measure of the decay of a contaminant in the human wake, the intensity of laser light incident on the photodiode is assumed to be inversely proportional to the concentration (i.e. the optical density) of theatrical fog in the wake. Theoretically, the linearity of the transmittance may fall off due to multiple scattering at high concentrations. However, the subject was not heavily seeded in these experiments. Thus, for present purposes, the linear assumption is appropriate.

As shown in Fig. 3, the decay of a body contaminant in the human aerodynamic wake is roughly exponential in nature. Moreover, the concentration is highly dependent on the vortex shedding phenomenon, as illustrated by a representative individual experimental trial plotted in Fig. 3, where periodic peaks in concentration associated with the shedding

of large-scale turbulent vortices are observed downstream of the walking subject, superimposed on a general exponential decay. However, in these data, the effect of vortex shedding is essentially “averaged out,” resulting in a relatively-smooth ensemble-averaged contaminant decay curve.

Lastly, we note that the time duration or time extent of the contamination in the human wake (the elapsed time during which significant contaminants are observed from a fixed point as the wake passes), taken here as the time to reach 10% of the initial concentration, is approximately 3 seconds. That is, a collection time of about 3 seconds is necessary to acquire the majority of a body contaminant present in the aerodynamic wake downstream of a walking person.

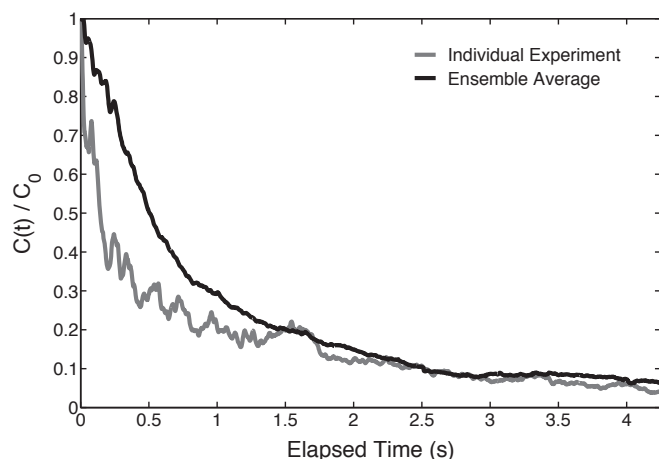


Fig. 3. Decay of a passive-scalar body contaminant in the human aerodynamic wake measured as concentration of theatrical fog downstream of the walking human subject for a representative experimental trial and the ensemble average of 30 experiments. The data are normalized by C_0 , the initial concentration of theatrical fog in the wake. Individual experiment results varied slightly due to the unsteady vortex shedding around the body and small variations in walking speed, thus the ensemble average of 30 experiments is also presented.

IV. DESIGN OF A HUMAN AERODYNAMIC WAKE COLLECTOR

To collect the human aerodynamic wake for subsequent analyses, there are two approaches: active and passive wake collection. Active collection involves either pushing or pulling (i.e., drawing in) the wake toward a collector inlet as a person walks past. We explore the use of turbulent air jets for actively pushing or directing (vectoring) the wake flow shortly. However, potential flow inlets have a limited aerodynamic “reach,” defined as the distance from the inlet within which air is captured [16, 17]. Consequently, using active wake collection alone via drawing the wake flow toward a collector inlet (e.g., using a blower) over large distances is impractical, as it would require exceedingly large airflow rates. Additionally, if the collector inlet is not located in line with the direction of the wake flow, then the inlet suction must also overcome the tangential component of momentum associated with the human wake.

Passive wake collection, on the other hand, utilizes the inherent momentum of the wake to facilitate its collection.

From a Lagrangian point-of-view, the human wake consists of shed vortices and other turbulent wake structures that *follow* a walking person with significant momentum. Thus, if a walking person makes a moderately-abrupt turn, the inertia of the wake will carry it forward even though the human subject has turned in a different direction. Such an approach may be used to separate the aerodynamic wake from a walking person and to collect it for chemical trace analysis.

The present study uses a combination of both active and passive techniques to efficiently collect the human aerodynamic wake. Specifically, a systematic experimental study was carried out in the design of a human aerodynamic wake collector that utilizes the inherent momentum of the wake as the primary means for collection, augmented by active approaches (suction applied to the collector inlet and wake vectoring via turbulent air jets) as secondary means for enhancing wake collection efficiency. An overview of the design process is provided that includes the specification of critical design parameters through a large series of parametric experiments that varied several components of the collector design including: portal width, use of entrance fairings, subject turning angle, collector orifice location and dimensions, collector inlet contraction design, and use of turbulent air jets for both active wake collection and for liberating chemical trace signal from a walking person. Due to the broad scope of the present study, some details of the design process are omitted. Pertinent references are provided that include several student theses (e.g., [18, 19]), which thoroughly document the methodology and results of this extended research program.

A. Portal Width

To separate the aerodynamic wake from a walking person, a subject must be required to negotiate a moderately-abrupt turn without “cutting the corner.” Thus, to force passengers to walk through the full turning angle, a minimum practical portal width of 0.73 m (28.75 inches) was chosen, based on recommendations from TSA Human Factors personnel [14].

B. Entrance Fairings

Flow entrances, such as that to the present chemical trace detection portal, should not have abrupt changes in geometry. Sharp corners result in the formation of a “vena contracta,” where inlet vortices reduce the effective cross-sectional area of the entrance, causing increased flow impedance. To eliminate the formation of a vena contracta, entrance fairings may be used with an optimal radius such that the contour of the fairing follows the streamline curvature of the inlet flow. According to Bleier [20], the radius of inlet fairings should be $0.14D$, where D is the diameter of the duct. Using this guideline, where D was taken as the hydraulic diameter of the portal entrance, inlet fairings of radius 0.15 m were designed to smoothly direct the aerodynamic wake of a walking person into the chemical trace detection portal.

To examine the effectiveness of the fairings, laser light sheet flow visualization experiments were carried out with and without entrance fairings attached to the portal entrance. As illustrated in Fig. 4, the use of entrance fairings was shown

to prevent the formation of a vena contracta. Accordingly, entrance fairings are required to maximize the flow rate of the contaminant-laden wake that enters the chemical trace detection portal behind a walking person.

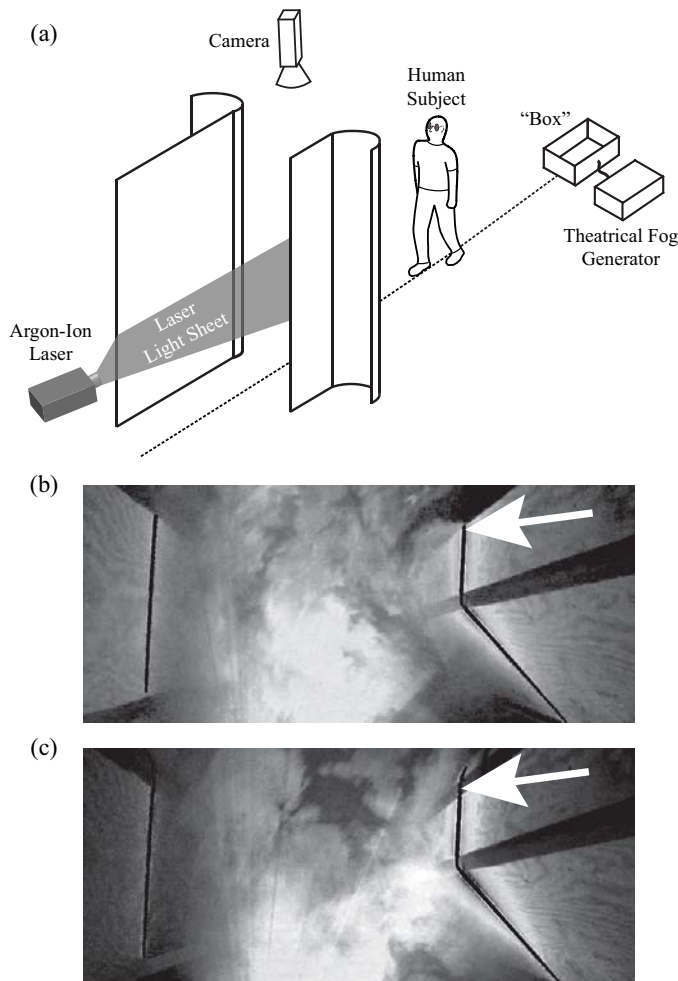


Fig. 4. (a) Schematic illustration of laser light sheet flow visualization experiments used to observe the human aerodynamic wake flow in the portal entrance without (b) and with (c) inlet fairings. The arrow indicates the portal entrance, where the absence of inlet fairings results in the formation of a vena contracta (b) and the inclusion of entrance fairings is shown to prevent the formation of a vena contracta (c).

C. Optimal Turning Angle

From a fluid dynamics point-of-view, a 90° turn would be ideal, if a person were capable of negotiating such a maneuver without pausing. However, from a human factors perspective, this is impractical, especially with a brisk walking pace. Thus, turning angles of 45° , 60° , and 75° were examined using laser light sheet flow visualization (see Fig. 5).

The results show that, both aerodynamically and from a human factors point-of-view, a 75° turn is not advantageous. The subject in our experiments had difficulty negotiating this turning angle. Instead of walking through portal while making a continuous 75° turn, he came to a stop, pivoted, and proceeded out of the portal at the appropriate angle. In doing so, his aerodynamic wake impinged upon his back. Thus, a portion of the wake was prevented from being collected.

Alternatively, 45° and 60° turns are nearly identical in terms of human-wake behavior. There is no significant difference in the flow visualization footage between the two experiments. Thus, since a 45° turn is easier to negotiate, it is selected as the optimal turning angle. Using a calibration length in the flow visualization footage, the typical radius of turn taken by the subject through for a 45° turning angle was measured to be 0.53 m.

A series of images from the flow visualization experiments showing the subject walking through a 45° turn is shown in Fig. 5. The wake's momentum clearly carries it through the notional collection plane (the vertical plane which includes the illuminated nylon string). The wake collection orifice will later be located in this plane.

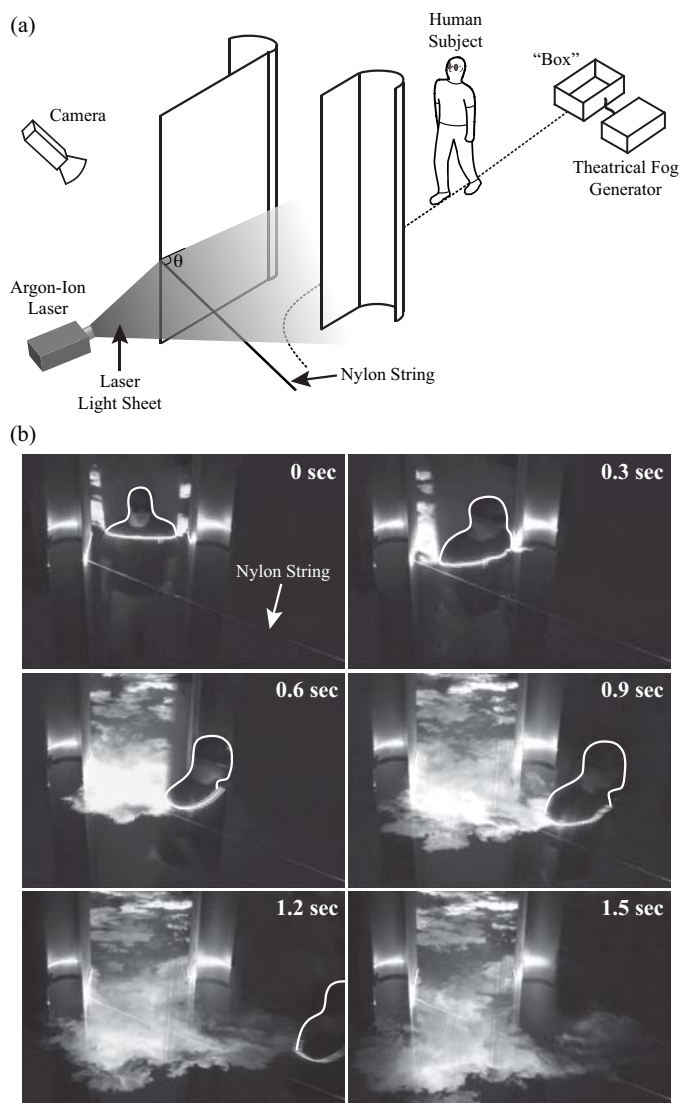


Fig. 5. (a) Schematic illustration of laser light sheet flow visualization experiments used to investigate the optimal human subject turning angle. (b) Sample laser light sheet flow visualization images of a human subject walking through the chemical trace detection portal and negotiating a 45° turn. Beginning at 0 sec, the human subject enters the portal walking toward the observer then turns to the observer's right through a 45° turn. After the human subject turns, the aerodynamic wake, which is seeded with theatrical fog, is observed to continue in the forward direction through a notional wake collection plane, visualized with an illuminated nylon string.

D. Wake Collection Orifice

1) *Design*: The size and location of the collector orifice was determined based on the foregoing flow visualization experiments. In this case a vertical wall stands such that it includes the illuminated nylon string shown in Fig. 5. The collector orifice is a rectangular orifice in this wall which must be sized appropriately to allow the passage of a majority of the human wake volume flux.

From laser light sheet experiments conducted at heights above the ground of less than 0.74 m (29 inches), a significant reduction in the strength of the human wake in these regions was observed. This is in accord with Edge's CFD simulation of the wake that showed the formation of a jet between the legs of a model human, which reduced the strength and coherence of the wake downstream of the legs [9, 5]. Thus, the bottom of the collector orifice is chosen at approximately 0.74 m (mid-thigh height). Above 0.74 m, as the subject makes a 45° turn, a small portion of the wake remains attached to him, but the bulk of the wake detaches from the subject and its inertia pushes it across the collection plane. From the experiments presented in this section, a collector orifice of the following dimensions was specified and used: height = 0.61 m (0.74 - 1.35 m above floor level), width = 1 m. The location of the orifice is shown in Fig. 6.

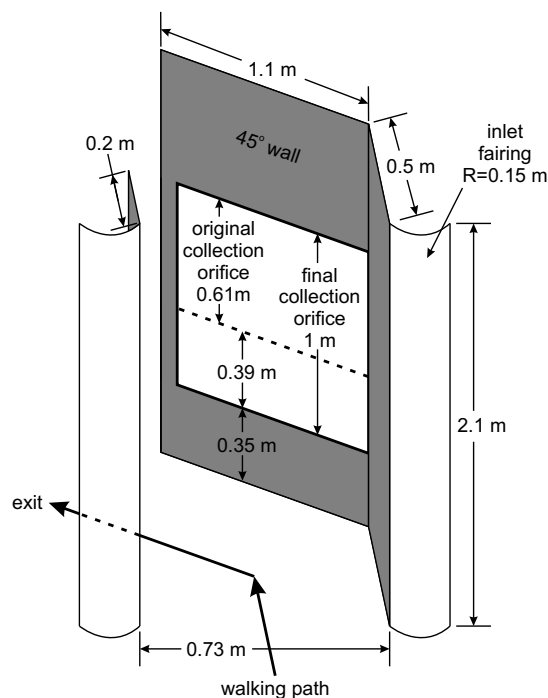


Fig. 6. Schematic of the wake separator, viewed from the portal entrance, showing the collection orifice location. The original collection orifice was enlarged in the final design to enhance performance for varied human subject height and lower-body collection.

2) *Contaminant Decay*: Contaminant decay measurements, as described in Section III-B, were also performed across the collection orifice. These experiments were conducted to determine the required sampling time after the wake separates from the subject and enters the collection orifice. Figure 7b is a plot of this measured contaminant concentration versus

elapsed collection time. Here, $t = 0$ is the collection initiation time: the time at which a nonzero contaminant concentration was first obtained in the experiment. This corresponds approximately to the time at which the subject makes the 45° turn. Thus, in practice, wake collection may be triggered as the subject passes this location.

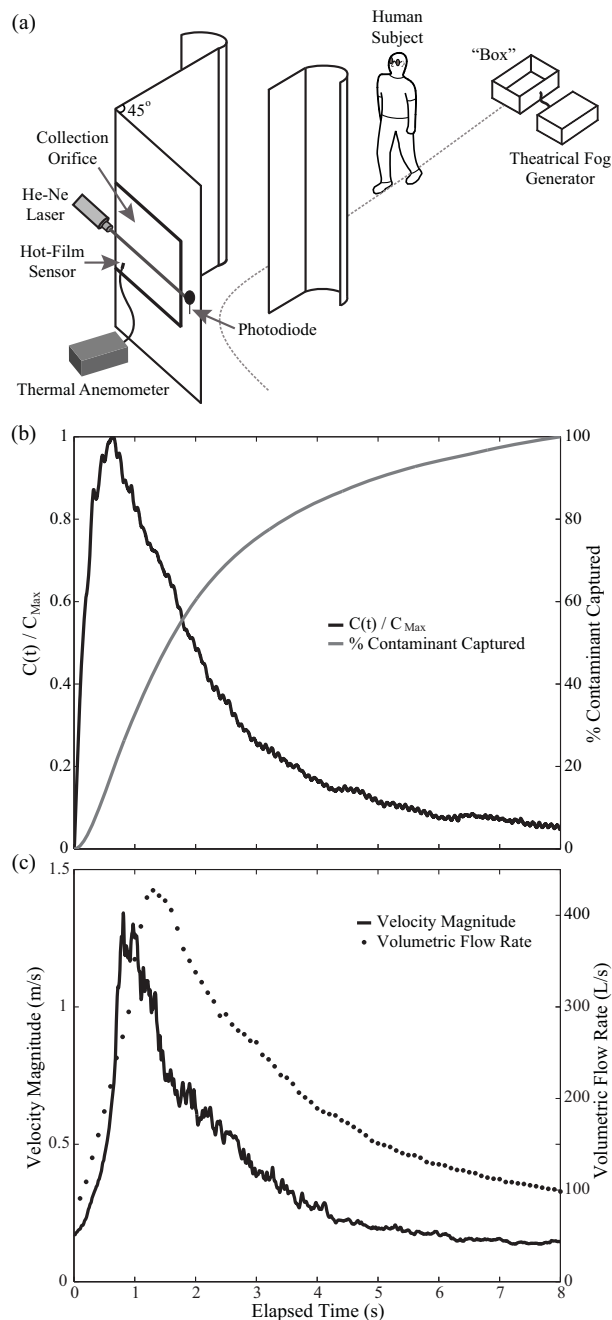


Fig. 7. (a) Schematic of the experimental setup used to measure the contaminant decay and flow rate through the collector orifice (b) Contaminant decay results (ensemble average of 39 trials, data normalized by C_{max} , the maximum concentration obtained in each trial) (c) Velocity/volumetric flow rate results (A typical ensemble average velocity as a function of time at one location in the collector orifice; The volumetric flow rate of the human aerodynamic wake through the collector orifice as calculated from integrating the ensemble average velocities at each location in the orifice)

As the subject walked through the portal and made the 45° turn, his wake separated from him and its inertia pushed

it through the collector orifice. This explains the initial rise in concentration seen in Fig. 7b. The average time to reach maximum concentration is, from the figure, 0.63 seconds. Upon reaching a maximum, the contaminant concentration decays in an exponential fashion, similar to that observed in the wake downstream of a person walking in a straight line (shown earlier in Fig. 3).

To obtain a measure of the total amount of signal captured for sampling, the normalized concentration versus time curve in Fig. 7b was integrated at each discrete time interval to yield the total contaminant captured through the collector orifice as a function of elapsed collection time. The results of the integration are shown in Fig. 7b on the right axis, from which we see that 75% of the total available signal can be collected after 3 seconds elapsed collection time. This establishes a minimum permissible separation between subjects that may be used to estimate maximum passenger throughput, though longer separation times may be required in practice to achieve aerodynamic separation of consecutive passengers and for the desorption and analysis of the trace chemical signals.

Since all of our experiments were conducted using a single human subject, the question of the effect of subject height on collection of the wake arises. However, as demonstrated in Edge's CFD simulation of the human aerodynamic wake, where a point contaminant was released from the abdomen of a model human, due to turbulent mixing the contaminant is rapidly mixed to a nearly uniform distribution in the wake [9, 5]. Thus, provided that a fraction of the subject's torso is within the vertical extent of the collector orifice, a sample of the contaminant in the wake will definitely be captured.

3) *Volumetric Flow Rate:* The volumetric flow rate through the collection orifice after a subject walks through the wake collector was measured using hot-film anemometry. 300 individual experiments were performed to develop statistically significant measurements of the flow rate through the collection orifice. Figure 7a shows the experimental setup used here.

A hot-film anemometer was used to take velocity measurements at 20 different, evenly-spaced locations in the plane of the collector orifice. An ensemble of 15 measurements was taken at each location, at a 250 Hz data rate for 8 seconds elapsed time. The volumetric flow rate of the portion of the wake passing through the collector orifice was then determined by numerically integrating the velocity data over the inlet area of the orifice, for the 8 seconds of data with increments of 0.1 second.

Figure 7c is an example of the ensembled velocity data at one location. Note the initial rise and subsequent exponential decay, which was also observed for the contaminant concentration in Fig. 7b. Additionally, Fig. 7c shows the result of the integration over the collector orifice, where the flow rate of the human aerodynamic wake through the collector orifice peaks at 427 L/s.

After these experiments, it was determined that the collection orifice in the final design should be enlarged to accommodate a wider range of human subjects. The final design used a collection orifice with a width of 1 m (the same as the experiments) and a height of 1 m. The orifice opening had the same top height, and was extended downward because

the test subject used here was of above average human height. Enlarging the orifice downward also improves collection of particles released from a subject's shoes. The final orifice design also required a larger volumetric flow rate of 750 L/s to maintain the flowrate over the original portion. This flow rate was used in the design and testing of the air mover and impactor.

E. Aerodynamic Contraction Design

A simple aerodynamic contraction was designed for reducing the cross-sectional area of the air path from the collection orifice to the inlet to the inertial impactor used for the sample collection (see Section V). The design of the aerodynamic contraction was based on the principles described by Su [21]. It converged the captured wake flow to the impactor with minimum pressure losses. The final design reduces the collection orifice area of 1 x 1 m to 0.305 x 0.305 m with a smoothly varying curve. Computational simulations using FLUENT software predicted the pressure loss to be 42 Pa for a flow rate of 750 L/s.

F. Air Mover for Human Wake Collection

A Cincinnati Fan SPB-15 3.75kW blower with a variable frequency drive was used to provide the motive force for the captured aerodynamic wake, and to overcome the pressure losses through the contraction and inertial particle impactor. The power and flow requirements used to specify this blower are further discussed later in relation to the inertial impactor needs.

A simple conical diffuser, with a 15° angle, was attached to the outlet of the air mover. This diffuser helps to reduce outlet pressure losses of the blower and improves the overall performance. The diffuser was approximately 1 m long, with an exit area of approximately 0.4 m.

G. Turbulent Air Jets

Turbulent air jets ("puffers") were explored for their potential to enhance chemical signals removed from a subject and for the ability to vector the wake flow toward the ultimate collection location. These turbulent jets, also called "puffer jets," are widely used in other chemical trace detection applications (e.g., [22]). For the present studies the jets were converging nozzles of 4.55 mm exit diameter, with a typical stagnation pressure of 552 kPa (80 psia), resulting in $Re \sim 371000$.

Flow visualization experiments showed that the air jets that impinged on the human subject had no noticeable influence on the behavior of the human aerodynamic wake as it crosses the collection plane. Thus, impinging jets can be used to enhance signal generation from a subject without affecting the wake transport. In contrast, air jets that were aimed at the back of the subject significantly vectored the wake itself. If these jets are properly oriented, they are capable of pushing the wake into the collection region.

As a result of the flow visualization experiments, we conclude that puffer jets may be used for two different and independent purposes in the trace detection portal: signal enhancement and wake vectoring.

In using puffer jets for signal enhancement, the location of the jets must be far enough upstream such that any signal released from the subject is allowed sufficient time to become entrained in the trailing wake. A theoretical analysis was conducted assuming potential flow around the subject's body to estimate the optimal upstream puffer jet location. In summary, a particle that is released from the clothing on the front of the subject, along the centerline, is estimated to reach the wake in approximately 0.7 seconds. Given the baseline walking speed of 1.34 m/s, the puffer jet(s) should therefore be positioned 0.9 m upstream of the collector orifice. More details on experiments involving turbulent air jets for signal enhancement can be found in [19].

V. INERTIAL PARTICLE IMPACTOR

An inertial particle impactor was chosen as the most appropriate device for collecting and analyzing micron-range particles present in the high-volume wake of a walking person. The present impactor design was constrained by the flow characteristics of the human aerodynamic wake, as discussed previously, and the need to collect particulate for trace chemical detection. The design volumetric flow rate is 750 L/s to accommodate capturing the entire peak wake flow rate. Based on published trace-explosive contamination studies [23], the design 50% cutoff particle was established as a 5 μm diameter particle with a density of approximately 1620 kg/m^3 .

A. Background

Inertial particle impactors are important tools for removing particles from airstreams. These devices incorporate a wide variety of geometries and flow characteristics, but all collect particles on the simple basis that airborne particles have more inertia than the airstreams that carry them [24, 25].

The basic science of inertial impactors has been thoroughly developed by Marple and collaborators [26, 27, 28, 29, 30, 24], and is well understood from their work. In its most basic sense, an impactor contains a nozzle for accelerating the particle-laden airflow to form a jet, and a plate upon which the resulting jet impinges. The plate is positioned perpendicular to the impinging airstream, thus forcing the air to divert around it. The nearly-massless air molecules move around the plate with no consequence beyond a characteristic pressure drop. Particles in the airstream, however, with significantly more inertia than the air, cannot negotiate the sharp turn around the plate and thus "impact" upon the plate surface. The impacted particles are thus removed from the airstream based on the geometry of the impactor and the particle characteristics. A fraction of particles within the airstream may also be too small and have insufficient mass to be impacted, and instead follow the air streamlines and remain within the airstream [26].

Other impactor flow geometries exist, such as virtual impactors [31] and centrifugal impactors [25], to collect particles in a different manner than upon a simple impaction plate. These are not relevant to the present work. Cascade impactors [32], which collect particles of different sizes incrementally on sequentially impaction plates are also not relevant here.

Impactors are used in a variety of applications including air filtering and air pollution sampling. Most of these devices are designed to collect particulate samples in a certain location for analysis to determine particle size, concentration, and chemical composition [33, 34, 35, 36]. Most existing designs operate at very low airflow rates (0.01 - 5 L/min) and are aimed at a specific narrow range of particle sizes. Most literature references to "high-volume" impactor designs are in the flow rate regime up to 100 L/min [37], which is an order of magnitude lower volume flow rate than that required in the present application. Rapid, high-volume collection of a wide particle size range in a single impaction step is uncommon in the literature, and in impactor technology in general.

B. Impactor Design

The impactor design process began with a simple conceptual geometry [26, 25], which was then streamlined through an iterative computational procedure. The resulting design is unique in terms of its fluid-dynamic design, high-volume throughput, and particle capture capability.

1) *Theoretical Design*: The basic geometry of an impactor is well-defined for capturing particles of a known size [26, 29, 30]. The basic geometry ratios, as a function of jet throat width, W , determined by [29] have been used as a starting point here and are shown in Figure 8a. Whether a given particle is impacted (collected) is governed by the impactor geometry along with characteristics of the particle and the encompassing airstream defined by the Stokes number.

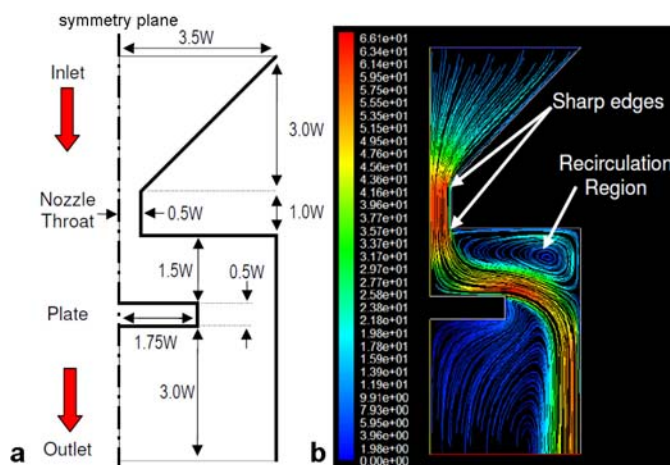


Fig. 8. Initial impactor design with (a) theoretically-ideal geometry ratios from [29] and the (b) computationally-generated steady-state streamlines through the geometry colored by local velocity magnitude (m/s). The domain shown represents half of a symmetric impactor geometry, where the centerline of the impactor is the symmetry plane. The identified recirculation regions and sharp corners are undesirable in terms of pressure loss, and are eliminated by a subsequent streamlining process.

The non-dimensional Stokes number, Stk , is a ratio of a particle's relaxation time to a characteristic flow timescale which describes impaction characteristics well [38, 29]. As given in Equation 1, the Stokes number is a function of a particle's density ρ_p , diameter D_p , and Cunningham slip factor C (assumed to be $C = 1$, for more discussion of the choice in value of C see [29]), along with the volumetric flow rate Q

of air with viscosity μ , density ρ_a , and average velocity u_{ave} through an impactor with a throat width W and length L .

$$Stk = \frac{\rho_p u_{ave} C D_p^2}{9\mu W} = \frac{\rho_p Q C D_p^2}{9\mu L W^2} \quad (1)$$

Impactor design theory shows that the cutoff Stokes number is dependent upon the jet Reynolds number and impactor geometry [26], but in general it can be assumed that particles with a Stokes number greater than 1 will impact, while those with a smaller Stokes number will usually remain in the airstream. Using a design Stokes number of 1 and a certain particle density, the “cutoff diameter” for an impactor can be estimated from Equation 1 [29]. In practice, the flow uniformity at the jet nozzle exit and the particle location relative to the impactor centerline also affect impaction, thus some particles with $Stk < 1$ will impact and some with $Stk > 1$ will remain in the airstream and pass through the device or impact with a reduced efficiency.

One advantage of particle impactors over particle filters is that impactors cause a smaller pressure loss for the same flow rate. The theoretical pressure drop, ΔP , across the entire impactor is approximately equal to the dynamic pressure, q , at the jet throat as estimated by [29]:

$$\Delta P \approx q = \frac{1}{2} \rho u_{ave}^2 = \frac{1}{2} \rho \frac{Q^2}{(LW)^2} \quad (2)$$

2) *Impactor Requirements and Design Space*: The overall size and particle cutoff diameter of the present impactor were established by its intended use: sampling particles from the aerodynamic wake of a walking person. A design-space study was conducted using Equations 1 and 2 with throat width W and bulk fluid flow rate Q as the independent variables and throat dynamic pressure q and impactor length L as the dependent variables.

The volumetric flow rate of the human aerodynamic wake through the enlarged collection orifice of 750 L/s sets a characteristic linear dimension, e.g. the side dimension L of the required impactor, on the order of 1 meter assuming a square cross-section (an order of magnitude larger is impractical and an order of magnitude smaller is approaching the compressible-flow regime). The performance specifications of commercially-available blowers, chosen based upon the volume flow rate of air, set the upper limit of permissible pressure drop across the impactor based upon the available electrical power (~ 4 kW). Designs having throat dynamic pressures above this level were removed from the design space. Designs having impactor lengths larger than 1 m were also deleted due to impracticality of fabrication and incompatibility with the scale of appropriate air-movers.

The design also dictated that the impactor length would have to be significantly larger than its width ($L \gg W$) in order to accommodate the large flow rate and maintain a small cutoff particle diameter. To facilitate this and to produce a practical design, a multiple-slit impactor [29, 39] design was chosen with three distinct, identical impactor slits, each of length L' .

These constraints lead to the final characteristics summarized in Table I. More details can be found in [19].

3) *Fluid-Dynamic Optimization of Impactor Design*: Using the baseline impactor design shown in Figure 8a, a computational optimization of the flow path was performed using the computational fluid dynamics (CFD) package FLUENT to simulate flow through the impactor. The computations were performed using a steady-state, two-dimensional domain with a symmetry condition on the impactor centerline, pressure inlet and outlet boundary conditions, and a standard k- ϵ turbulence model. The two-dimensional flow modeled the space shown in Figures 8b and 9 with an infinite depth (infinite impactor length L), which is appropriate for $L \gg W$. Flow symmetry permitted half of one slit to be modeled.

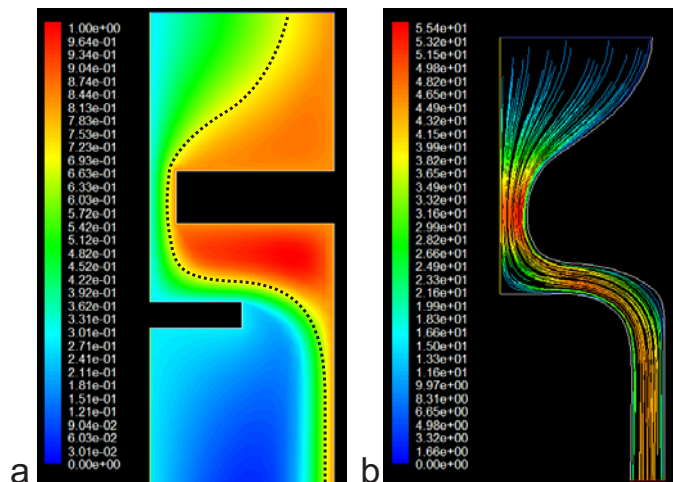


Fig. 9. (a) Contour plot of the stream functions (kg/s) for the flow in the impactor design. The dividing streamline is represented by the dotted line. (b) Streamlines colored by velocity magnitude (m/s) for the final streamlined impactor design.

The initial simulations using the geometry of Figure 8 revealed recirculation regions in the airflow path, as identified in Figure 8b. These recirculation regions have not been discussed in previous impactor studies, but they cause a significant pressure loss through the impactor. The calculated pressure drop across the initial impactor design (Figure 8) was approximately 7.02 kPa, which is significantly larger than the expected value (from Equation 2) of 2.19 kPa. Previous impactor studies and designs [27, 29] have focused on low-flow rate applications where pressure drop is not critical. For the present application, minimizing pressure losses is essential to limit blower size, and thus the impactor design must be streamlined. It was also essential to eliminate flow recirculation regions because small particles and vapors can become effectively “trapped” there in the impactor, which is undesirable for applications to aviation security (any such material needs to clear rapidly before the next human subject enters the system).

Streamlining of the impactor was first achieved by identifying the boundary streamline that distinguishes the bulk flow from regions of flow recirculation. The dashed line in Figure 9a represents one such dividing streamline. The coordinates of the dividing streamline were then used to create the new solid boundary of the impactor geometry. Through an iterative process, all of the separated flow regions were removed and the final attached-flow impactor geometry, as shown in Figure

TABLE I
FINAL IMPACTOR DESIGN PARAMETERS

Flow rate	Q	750 L/s
Design particle cutoff diameter	D_p	5 μm
Design particle density	ρ_p	1620 kg/m ³
Stokes number of design particle	Stk	0.99
Throat width	W	0.014 m
Throat total length	L	0.914 m
Individual throat length	L'	0.305 m
Impactor inlet area		0.093 m ²
Throat dynamic pressure	q	2.0 kPa
Calculated pressure drop	ΔP	0.54 kPa
Measured pressure drop	ΔP	0.85 kPa
Average jet velocity	u_{ave}	58.6 m/s
Jet Reynolds Number	Re	103000

9b, was achieved.

4) *Final Impactor Design*: The final impactor design contained three identical slits, each with $L' = 0.305$ m (12.0 in) and $W = 0.014$ m (0.57 in). The total impactor inlet is a square 0.305 x 0.305 m area with a volumetric flow rate of 750 L/s, connected to the 3.75 kW air mover. The final design yields a Stokes number of $Stk = 0.99$ for the target particles as described earlier.

The final design was analyzed by CFD to verify the flow-geometry streamlining and to measure the total pressure drop, which is given in Table I. The resulting flowfield showed that the division into three slits did not adversely affect the performance of the impactor and only increased the calculated pressure drop minimally. There was almost no flow separation in critical areas upstream of the impactor face, and the computed pressure drop was well below the head provided by the blower. Some minimal separation exists downstream of the impactor surface, which is impractical to eliminate without a very-long outlet diffuser.

The final calculated impactor pressure drop is less than the throat dynamic pressure q (Equation 2). The pressure drop through the streamlined impactor was an order of magnitude smaller than the pressure drop through the initial geometry (Figure 8a) which was calculated to be 5.48 kPa.

A summary of the final impactor design parameters is given in Table I, and an image of the final three-slit impactor design is shown in Figure 10.

The final impactor design was manufactured from solid aluminum and built into the wake collector device used for the experiments described in Section IV [19, 18, 40]. The experimental analysis discussed below was conducted on the impactor once installed in the portal device, but the analysis is specific to the impactor at its design airflow rate and is independent of the wake collector apparatus in general.

C. Experimental Measurements of Impactor Collection Efficiency

To validate the streamlined impactor design, experiments were performed to determine the locations where particles impacted on the impactor surface and to estimate the collection efficiency.

Various methods have been reported in the literature for measuring the efficiency of inertial impactors. Typically the

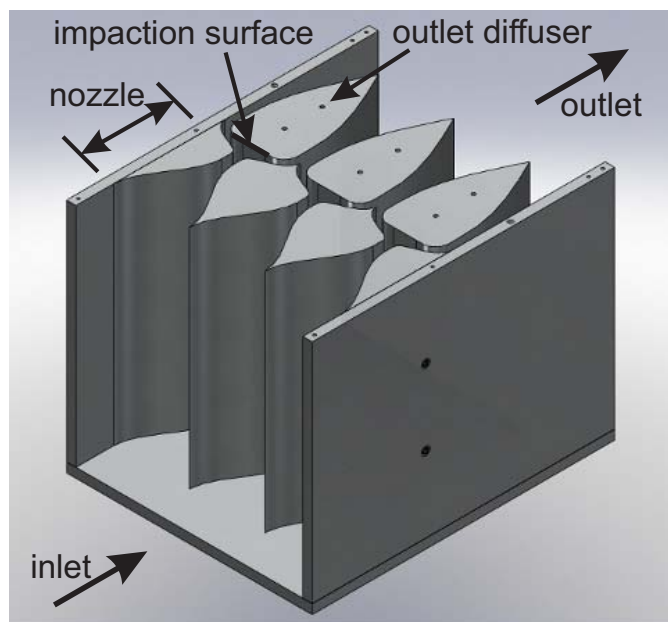


Fig. 10. Final impactor design with the top surface removed to show the details of the three-slit design. The inlet is closest in the view with flow moving in the direction shown.

efficiency is measured by releasing a known number of particles upstream of the impactor and measuring the fraction of particles that are collected [25, 41, 42]. These techniques, however, could not readily be applied here due to the unique impactor geometry, size, and airflow rate. Instead, the analysis included an experimental aerosol analysis method and an experimental microscope-based study of impacted particles.

1) *Experimental Aerosol Study*: The first set of experiments indirectly measured particle impactation by analyzing aerosol particle size distributions upstream and downstream of the impactor. This approach has been used by other researchers, including [43].

These experiments began with the generation of an aerosol of talc powder upstream of the impactor inlet using a fluidized bed device. The size and flow rate of this impactor required a large volume of aerosol as the input to each test, thus talc was chosen for its low cost, ease of use, and particle size range. The talc powder provides a poly-disperse particle size distribution that allows impactor characterization over a wide range of Stokes numbers in a single test.

A Malvern SprayTec aerosol sizer was used to analyze the talc aerosol upstream (before) and downstream (after) of the impactor. This Fraunhofer-diffraction-based device measures the particle size distribution of an aerosol in terms of percent volume as a function of particle size. The upstream aerosol size distribution was measured first to identify the particle distribution that entered the impactor. The size distribution as a function of Stokes number is shown in Figure 11a. The talc powder used here has a density of 2800 kg/m³, which yields a 4 μm diameter particle at $Stk = 1$. The measured upstream aerosol size distribution was also compared to a laser-diffraction size distribution of the same powder that was performed with a benchtop instrument and particles in solu-

tion. This comparison showed that the fluidized-bed aerosol generator was sufficiently de-agglomerating the talc powder, producing an aerosol size distribution that was approximately equal to the wet benchtop measurement [18]. Although de-agglomeration was performed, no charge neutralization was attempted, which could contribute to some of the experimental errors.

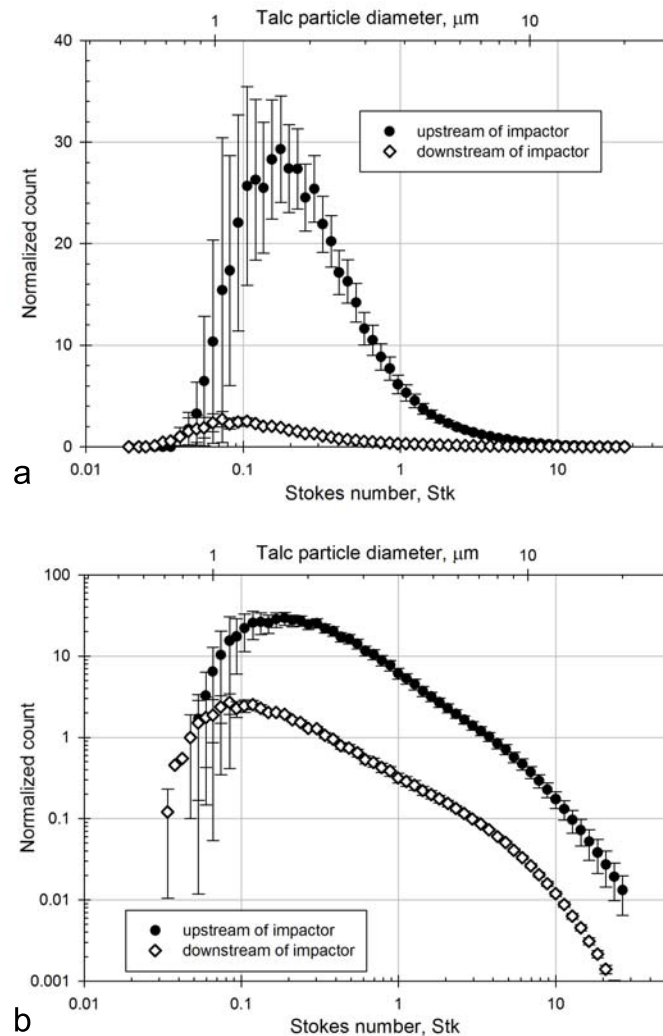


Fig. 11. Measured and normalized aerosol particle size distributions upstream and downstream of the impactor with (a) linear and (b) logarithmic vertical scales. Each data set represents the average of 10 experiments, with the standard deviation given as the error bar. These data are normalized by assuming that the number of small ($Stk = 0.04$, $0.8 \mu\text{m}$ diameter talc) particles present upstream and downstream is the same. The logarithmic scale shows that the upstream and downstream aerosols have different Stokes numbers at which the maximum count of particles occurs. The shift in this peak indicates that larger particles are being removed from the airstream.

By analyzing the aerosol particle size distributions before and after the impactor, impaction characteristics can be extracted. As presented in Figure 11a, the particle size distributions are significantly different across the impactor. The differences between the curves are difficult to interpret in Figure 11a in terms of a particle collection efficiency due to their presentation as a normalized count. The results are thus converted to a relative particle count to define collection efficiency.

An initial sample volume of 1 m^3 of air containing talc particles is arbitrarily assumed for each data set in Figure 11a. From this the particle volume fraction is converted to a number of particles. The data are then normalized to each other by assuming that the smallest particles measured will pass through the impactor unaffected. The number of small ($Stk < 0.04$) particles present in the volume upstream of the impactor should therefore be the same as the number of these particles present after the impactor. This assumption is affected by any impaction of these small particles, but that would cause the measured efficiency from this analysis to increase, thus this approximation provides a conservative estimate of the impaction efficiency. The data after this normalization are presented in Figure 11.

This analysis could also be affected by the presence of airborne talc particle agglomerations upstream of the impactor, that are subsequently broken up while passing through the impactor. If such agglomerations existed upstream but broke up through the impactor to release smaller particles downstream, this would cause an apparent lowering of the calculated cutoff diameter. In order to evaluate this issue, the talc aerosol particle size distribution upstream of the impactor was compared to the size distribution of de-agglomerated talc in a wet-particle laser measurement of the talc used to make the aerosol. These particle distributions matched well in terms of overall range of particle diameter, average diameter, and most often occurring diameter, and are shown elsewhere [18].

Figure 11b clearly shows that the impactor is removing particles from the airstream with Stokes number $Stk > 0.05$. It also shows that the Stokes number at which the maximum number of particles is observed decreases from upstream to downstream. This indicates that large particles are selectively being removed from the airstream, as expected.

These data were converted to an estimated impactor efficiency curve, which is presented in Figure 12. The uncertainty in the aerosol measurement technique was large, and thus there is a large error bar on the efficiency estimate, but nevertheless we estimate the 50% cutoff Stokes number at $Stk \sim 0.2$. This cutoff Stokes number is small compared to other impactors reported in the literature [29], but is believed to be accurate and a result of the high Reynolds number for this impactor and its unique contouring.

The cutoff diameter can also be estimated as described by Zhang[44], using the following equation:

$$d_{50} = \sqrt{\frac{9\mu W}{\pi\rho_p C u_{ave}}} \quad (3)$$

which results in $d_{50} = 2\mu\text{m}$ ($Stk = 0.32$) for the present geometry. This value is within the error of the experimental measurements and supports this characterization of a very small cutoff Stokes number for this geometry.

2) *Experimental Particle Impaction Study*: Another experimental study was performed to directly examine particle impaction characteristics by measuring the locations where different-sized particles impacted. For these experiments the impaction plate surface was covered with microscope slides onto which the particles were impacted, as shown in Figure

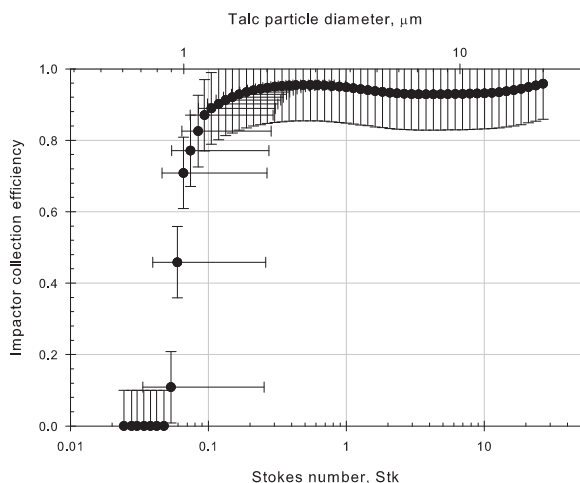


Fig. 12. The experimentally determined impactor removal efficiency as a function of Stokes number. The large error bars here are due to the experimental methods used.

13. After impactation the slides were removed and examined under a microscope. The primary variable of interest in this study was the location and distribution of impacted particles as a function of particle size.

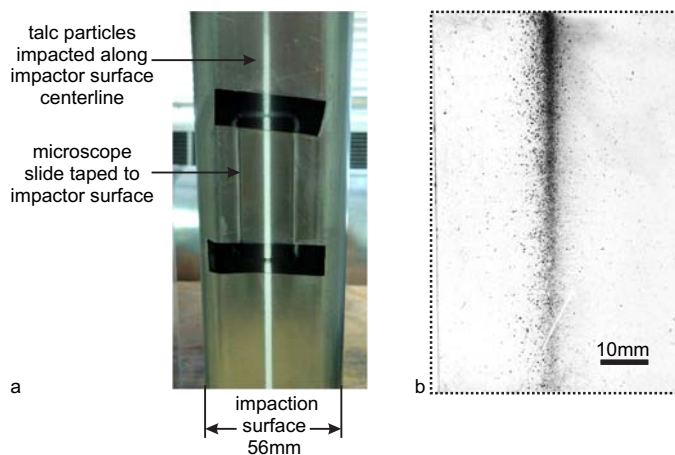


Fig. 13. (a) Image of talc impactation on a microscope slide and on the impactor plate surface. This image was recorded after an experiment where significantly more talc was injected than needed for the measurement. (b) Image of a microscope slide with impacted talc particles at a density typically used for the measurements presented. Note that the image illumination is non-uniform and thus appears to show a non-uniform vertical distribution of particles along the slide, which was not actually observed in the experiments here.

Before the full analysis was conducted, experiments were performed to determine the influence of the microscope slides on impactation characteristics. The addition of the microscope slides slightly changes the distance between the impactor throat and impactation plate, which could affect collection efficiency. Also impactation, bounce, and blow-off characteristics of the particles might be affected by differing impactation substrates. Experiments were performed using the above-described aerosol analysis to analyze the downstream particle distributions for the impactor with the bare aluminum impactor surface, double-sided tape, and microscope slides. The results

showed no significant variation in the downstream particle distributions as a function of substrate (within the existing experimental errors), although other researchers have observed such variations in collection efficiency (e.g., [41]).

Preliminary experiments were also performed to analyze variations in the impacted particle distributions across each of the three impactor slits and along the length of each slit. The experiments showed that there was no significant variation with these parameters [18]. The center of the middle impactor slit was therefore used to collect the following experimental data, which were averaged over a 0.075 m length and over multiple experiments.

For each experiment a microscope slide was attached to the impactor plate surface along the centerline and then a limited amount of the talc aerosol was injected upstream of the operating impactor. Only enough aerosol was injected so that a sufficient number of particles was collected on the microscope slide for meaningful statistics, without increasing the probability of particle-particle interactions on the surface. The typical amount of talc collected is displayed in Figure 13b. To inject only a limited amount of the aerosol, the aerosol generator had to be pulsed rapidly, which may have altered the size distribution of talc released. The aerosol pulse was too small to measure with the aerosol measurement equipment used above, so the size distribution was not known precisely. The results of the particle collection are therefore presented as a normalized count for each particle size, and no comparisons between impacted particle counts can be made. These data are used here only to show locations over which particles of different sizes are observed to have impacted.

Microscope images of the slides with impacted talc were processed with a simple MATLAB routine that identified individual particles in the images and then determined their size and distance from the impactor centerline. The measured particle sizes were binned in 0.5 μm diameter increments.

The results from the analysis of the microscope images are shown in Figure 14. They are an average of multiple experiments and show a normalized particle impactation count as a function of location for particles of varying Stokes number. The data are limited to a distance of 10 mm from the impactor centerline as this was the region of particular interest for this work.

The results in Figure 14 show that particles with larger diameters are impacted closer to the impactor centerline than are smaller particles. All particle sizes have a maximum impactation count along the centerline as expected along the stagnation streamline. The smallest particles, here with $Stk = 0.02$, have the widest distribution of particle impact locations. These particles cover the entire area examined and still have a high relative count at the edge of the observed region, indicating that there is still significant impactation occurring across more of the impactor surface. This is expected, as particles with smaller Stokes numbers will follow the fluid streamlines better and thus impact across a wider area. The particles with $Stk = 0.27$ are collected across the entire 10mm area examined, with almost no particles observed at the edge of this area, indicating that their impactation extent is about 10 mm from the centerline of the impactor. The larger particles

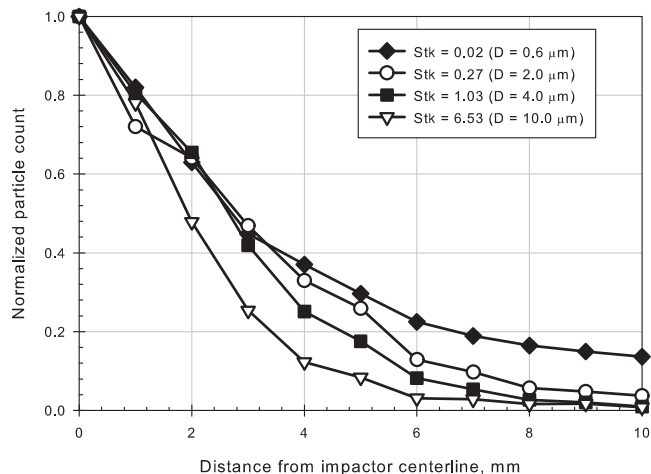


Fig. 14. Measured particle impact location relative to impactor centerline for varying Stokes number. The vertical axis represents the frequency of impaction counts at each location and is normalized by the number of particles captured on the impactor centerline for each particle size.

have a narrower distribution, with particles of $Stk = 1.03$ distributed over only 8 mm and those of $Stk = 6.53$ impacted only within 6 mm of the centerline.

These results cannot be directly converted to an efficiency curve because the frequency counts are arbitrary and the entire impactor surface was not measured. From the experimental data, however, it can be observed that the 50% cutoff point Stokes number is approximately between $0.02 < Stk < 0.27$, which agrees with the previous measurement. This small Stokes number cutoff is lower than, but on the order of, results presented elsewhere [29]. This difference in cutoff Stokes number relative to previously reported values is believed to be due to the significantly higher Reynolds number and streamlined design of the current impactor.

The excellent performance of the impactor in concentrating particles on its centerline has suggested a design feature for explosive particle detection in security screening. A 10 mm-wide slot along the impactor centerline is being used to impact particles directly upon a strip heater. The heater subsequently vaporizes any explosive particles directly into a detector [40].

VI. FINAL CHEMICAL TRACE DETECTION PORTAL DESIGN

The final design of the chemical trace detection portal is shown schematically in Figure 15. The system includes an “air puffer jet apparatus” which contains timing laser diodes and compressed air jets which impact the subject’s body on the front and back sides to release particles and thus improve detection. The back-side jets also help to vector the wake into the collector. The “wake separator” includes the 45° turning section and the collection orifice. The “aerodynamic contraction” reduces the flow area from the collection orifice to the impactor inlet area. The “impactor” removes trace chemicals from the airflow, which is driven by the “blower” which exhausts the airflow through the “diffuser”.

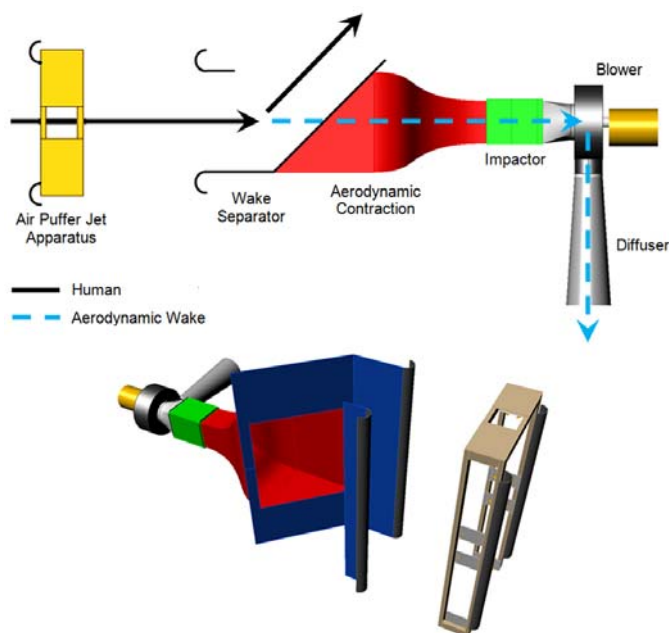


Fig. 15. Layout of the final chemical trace detection portal with top view and isometric view.

VII. PRELIMINARY RESULTS

Preliminary data have been collected to demonstrate the present wake-sampling chemical trace detection portal functionality. The preliminary experiments used “patches” of chemically-detectable materials located at specific locations on a human subject. This “patch testing” technique has been used previously to evaluate the performance of trace chemical detection portals [22].

The preliminary testing has shown that trace levels of chemicals can be detected from locations across the entire human body. The amount of collected material is a function of the pressure applied to the air jets and the location of the patches on the human subject. More trace signal was collected for higher-pressure air jets because the higher-pressure jets liberate more particles from the human subject [22, 45].

The collection of the trace chemicals was greater for patch locations on the upper body. This could be due to downward-vortex shedding from the shoulders of the walking human. For patch locations on the lower body, particle transport is more difficult in the upward direction needed in order to enter the collector, but the turbulent nature of the wake still allows some particles to be collected. Future improvements to this design may use directional air jets or a larger collection orifice to better collect particles from the lower body.

The preliminary experiments have shown no significant collection variations across the individual impactor plates or along their length. The turbulent mixing of the wake allows the particles to be nearly randomly distributed in the subject’s wake, thus the particle collection is relatively uniform across the impactor surface area.

The details of the validation of the impactor performance and the system performance in patch testing are available elsewhere [18, 19]. Additional information on the impactor and

the design of the automated, integrated IMS chemical detector was recently published by Fulghum et al. [40].

VIII. CONCLUSIONS

This paper has described a long-term research program for the development of a high-throughput chemical trace detection portal that is based on sampling the human aerodynamic wake. The primary conclusions of the work presented here are:

- 1) The buoyant human thermal plume was shown to transition to an advection-dominated aerodynamic wake at a walking speed of approximately 0.25 m/s.
- 2) The aerodynamics and dispersion characteristics of the wake were examined using laser-light-sheet flow visualization and spectrophotometry. We found that the human aerodynamic wake is highly turbulent and three-dimensional. The decay of a passive scalar downstream of a walking subject was shown to be exponential in nature.
- 3) Using the momentum of the human aerodynamic wake was shown to be a viable mechanism for airflow collection.
- 4) The flow rate of the human wake through the collector orifice was shown to be nearly an order of magnitude larger than current collection technology permits, requiring a high-flow-rate particle impactor that is larger than any currently published in the literature or commercially available.
- 5) A very-high-flow-rate particle impactor was designed using an iterative computational approach to streamline the impactor geometry in order to significantly reduce pressure drop and recirculation regions. This design process could be applied to any impactor, but is essential for high-flow-rate devices where limiting pressure loss is important.
- 6) The resulting impactor design was tested experimentally to identify particle impaction locations and particle capture efficiency. The results show a 50% cutoff Stokes number of $Stk \sim 0.2$, which is lower than any other reported in the literature. This is likely due to the high-flow rate design and streamlining of the flow passage.
- 7) Preliminary experimental testing with trace chemical patch sources has shown that the system is capable of collecting and detecting trace chemical contamination on human subjects walking through this system. The contamination can be detected from a range of source locations across the subject's body.

More details on this system can be found in several Pennsylvania State University theses [7, 19, 18] and a recent publication on the automation of the impactor's chemical detector [40].

ACKNOWLEDGMENTS

This research was funded by the US Department of Homeland Security under contract number CAA 06-G-032. It was performed at the Pennsylvania State University in the Gas Dynamics Laboratory of the Mechanical and Nuclear Engineering Department. The authors would like to thank J. D. Miller, L. J. Dodson-Dreibelbis, and the students of the Gas Dynamics Laboratory for their assistance.

REFERENCES

- [1] Anonymous, *Thermal Comfort, ASHRAE Fundamentals Handbook*, 2005.
- [2] A. J. Vander, J. H. Sherman, and D. S. Luciano, *Human Physiology: the mechanisms of body function*, 6th ed. McGraw-Hill, Inc., 1994.
- [3] B. A. Craven and G. S. Settles, "A computational and experimental investigation of the human thermal plume," *Journal Of Fluids Engineering-Transactions Of The Asme*, vol. 128, no. 6, pp. 1251–1258, 2006.
- [4] F. P. Incropera and D. P. DeWitt, *Fundamentals of Heat and Mass Transfer*, 5th ed. Wiley and Sons, Inc., 2002.
- [5] B. A. Edge, E. G. Paterson, and G. S. Settles, "Computational study of the wake and contaminant transport of a walking human," *Journal of Fluids Engineering*, vol. 127, pp. 967–977, 2005.
- [6] G. M. Rapp, "Convective heat transfer and convective coefficients of nude man, cylinders and spheres at low air velocities." *ASHRAE Transactions*, vol. 79, no. Part 1, pp. 75–85, 1973.
- [7] Z. M. Moyer, "The human aerodynamic wake and the design of a portal to sample it," Master's thesis, Mechanical and Nuclear Engineering Department, Pennsylvania State University, 2003.
- [8] A. Venzon, "Complementary CFD simulations and wind tunnel experiments for design of a walk-through explosives detection portal," Master's thesis, Mechanical and Nuclear Engineering Department, Pennsylvania State University, 2005.
- [9] B. A. Edge, "Computational fluid dynamics simulation of the human aerodynamics wake," Master's thesis, Mechanical and Nuclear Engineering Department, Pennsylvania State University, 2003.
- [10] L. S. Cohen and M. N. Director, "Transport processes in the two-dimensional near wake," *AIAA Journal*, vol. 13, no. 8, pp. 969–970, 1975.
- [11] P. K. Kundu and I. M. Cohen, *Fluid Mechanics*, 2nd ed. Academic Press, Inc., 2002.
- [12] G. S. Settles, "Chemical trace detection portal based on the natural airflow and heat transfer of the human body," US Patent 6 073 499, 2000.
- [13] —, *Schlieren and shadowgraph techniques: Visualizing phenomena in transparent media*. Springer-Verlag, 2001.
- [14] M. Snyder, "Human factors recommendations," personal communication, 2004.
- [15] G. F. Lothian, *Absorption spectrophotometry*, 3rd ed. Adam Hilger, Ltd., 1969.
- [16] R. J. Heinsohn and J. M. Cimbala, *Indoor Air Quality Engineering*. Marcel Dekker, Inc., 2003, pp. 517–580.
- [17] G. S. Settles, "Sniffers: Fluid-dynamic sampling for olfactory trace detection in nature and homeland security - the 2004 Freeman Scholar Lecture," *J Fluid Eng*, vol. 127, no. 2, pp. 189–218, 2005.
- [18] S. P. Frymire, "The development of a security-screening portal for human aerodynamic wake sampling," Master's thesis, Mechanical and Nuclear Engineering Department,

- Pennsylvania State University, 2009.
- [19] J. A. Volpe, "The design of an aerodynamic wake sampling portal," Master's thesis, Mechanical and Nuclear Engineering Department, Pennsylvania State University, 2007.
- [20] F. P. Bleier, *Fan Handbook: Selection, application, and design*, 1st ed. McGraw-Hill, Inc., 1997.
- [21] Y. Su, "Flow analysis and design of three-dimensional wind tunnel contractions," *AIAA Journal*, vol. 29, no. 11, pp. 1912–1920, 1991.
- [22] M. A. Thomas, "Aerodynamics of an explosive trace detection portal," Master's thesis, Mechanical and Nuclear Engineering Department, Pennsylvania State University, 2005.
- [23] J. R. Verkouteren, "Particle characteristics of trace high explosives: RDX and PETN," *J Forensic Sci*, vol. 52, no. 2, pp. 335–340, 2007.
- [24] V. A. Marple, "History of impactors - the first 110 years," *Aerosol Science and Technology*, vol. 38, no. 3, pp. 247–292, 2004.
- [25] V. A. Marple, B. A. Olson, and K. L. Rubow, "Inertial, gravitational, centrifugal, and thermal collection techniques," in *Aerosol Measurement: Principles, Techniques, and Applications*, 2nd ed., P. A. Baron and K. Willeke, Eds. Wiley-Interscience Inc., 2001, ch. 10, pp. 229–260.
- [26] V. A. Marple, "A fundamental study of inertial impactors," Dissertation, University of Minnesota, 1970.
- [27] V. A. Marple, B. Y. Liu, and K. T. Whitby, "Fluid mechanics of the laminar flow aerosol impactor," *Journal of Aerosol Science*, vol. 5, no. 1, pp. 1–16, 1974.
- [28] V. Marple and B. Liu, "On fluid flow and aerosol impaction in inertial impactors," *Journal of Colloid and Interface Science*, vol. 53, no. 1, pp. 31–4, 1975.
- [29] V. A. Marple and K. Willeke, "Impactor design," *Atmospheric Environment*, vol. 10, no. 10, pp. 891–896, 1976.
- [30] D. J. Rader and V. A. Marple, "Effect of ultra-stokesian drag and particle interception on impactor characteristics," *Aerosol Science and Technology*, vol. 4, pp. 141–156, 1985.
- [31] V. A. Marple and C. M. Chien, "Virtual impactors: a theoretical study," *Environmental Science and Technology*, vol. 14, no. 8, pp. 976–985, 1980.
- [32] V. A. Marple, B. A. Olson, and N. C. Miller, "A low-loss cascade impactor with stage collection cups - calibration and pharmaceutical inhaler applications," *Aerosol Science and Technology*, vol. 22, no. 1, pp. 124–134, 1995.
- [33] R. A. Gussman, L. C. Kenny, M. Labickas, and P. Norton, "Design, calibration, and field test of a cyclone for pm1 ambient air sampling," *Aerosol Science and Technology*, vol. 36, no. 3, pp. 361–365, 2002.
- [34] R. H. Brown and L. E. Monteith, "Gas and vapor sample collectors," in *Air Sampling Instruments for Evaluation of Atmospheric Contaminants*, 9th ed., B. S. Cohen and C. S. J. McCammon, Eds. American Conference of Governmental Industrial Hygienists, 2001, ch. 16, pp. 415–455.
- [35] V. A. Marple, K. L. Rubow, W. Turner, and J. D. Spengler, "Low flow-rate sharp cut impactors for indoor air sampling - design and calibration," *JAPCA-the International Journal of Air Pollution Control and Hazardous Waste Management*, vol. 37, no. 11, pp. 1303–1307, 1987.
- [36] C. Misra, M. D. Geller, C. Sioutas, and P. A. Solomon, "Development and evaluation of a pm10 impactor-inlet for a continuous coarse particle monitor," *Aerosol Science and Technology*, vol. 37, no. 3, pp. 271–281, 2003.
- [37] R. M. Burton and D. A. Lundgren, "Wide range aerosol classifier: a size selective sampler for large particles," *Aerosol Science and Technology*, vol. 6, pp. 289–301, 1987.
- [38] N. A. Fuchs, *The Mechanics of Aerosols*. Pergamon Press, 1964.
- [39] C. Misra, S. Kim, S. Shen, and C. Sioutas, "A high flow rate, very low pressure drop impactor for inertial separation of ultrafine from accumulation mode particles," *Journal of Aerosol Science*, vol. 33, no. 5, pp. 735–752, 2002.
- [40] M. R. Fulghum, M. J. Hargather, and G. S. Settles, "Integrated impactor/detector for a high-throughput explosive-trace detection portal," *IEEE Sensors Journal*, vol. 13, no. 4, pp. 1252–1258, 2013.
- [41] M. Chang, S. Kim, and C. Sioutas, "Experimental studies on particle impaction and bounce: effects of substrate design and material," *Atmospheric Environment*, vol. 33, no. 15, pp. 2313–2322, 1999.
- [42] L. C. Kenny and G. Liden, "A technique for assessing size-selective dust samplers using the aps and polydisperse test aerosols," *Journal of Aerosol Science*, vol. 22, no. 1, pp. 91–100, 1991.
- [43] C. Misra, M. Singh, S. Shen, C. Sioutas, and P. M. Hall, "Development and evaluation of a personal cascade impactor sampler (pcis)," *Journal of Aerosol Science*, vol. 33, pp. 1027–1047, 2002.
- [44] Y. Zhang, *Indoor air quality engineering*. CRC Press, 2005.
- [45] R. M. Young, M. J. Hargather, and G. S. Settles, "Shear stress and particle removal measurements of a round turbulent air jet impinging normally upon a planar wall," *Journal of Aerosol Science*, vol. 62, pp. 15–25, 2013.